Effect of Dust Extinction on Gamma-ray Burst Afterglows

 $\mathrm{Gu}\text{-}\mathrm{Jing}\ \mathrm{L}\ddot{\mathrm{u}}^{1},\ \mathrm{Lang}\ \mathrm{Shao}^{1,2},\ \mathrm{Zhi}\text{-}\mathrm{Ping}\ \mathrm{Jin}^{1},\ \mathrm{And}\ \mathrm{Da}\text{-}\mathrm{Ming}\ \mathrm{Wei}^{1}$

lang@pmo.ac.cn(L.S.)

ABSTRACT

In order to study the effect of dust extinction on the afterglow of gamma-ray bursts (GRBs), we carry out numerical calculations with high precision based on rigorous Mie theory and latest optical properties of interstellar dust grains, and analyze the different extinction curves produced by dust grains with different physical parameters. Our results indicate that the absolute extinction quantity is substantially determined by the medium density and metallicity. However, the shape of the extinction curve is mainly determined by the size distribution of the dust grains. If the dust grains aggregate to form larger ones, they will cause a flatter or grayer extinction curve with lower extinction quantity. On the contrary, if the dust grains are disassociated to smaller ones due to some uncertain processes, they will cause a steeper extinction curve with larger amount of extinction. These results might provide an important insight into understanding the origin of the optically dark GRBs.

 $Subject\ headings:$ gamma-rays burst: general—interstellar medium: dust, extinction

1. INTRODUCTION

Gamma-ray burst (GRB) is known as one of the most energetic stellar explosions in the universe. At present, the *Swift* satellite (Gehrels et al. 2004), a NASA mission dedicated to monitor this phenomenon, carries three instruments with separate wave bands: Burst Alert Telescope (BAT; $\sim 15-150$ keV), X-Ray Telescope (XRT; $\sim 0.3-10$ keV) and Ultraviolet/Optical Telescope (UVOT). BAT is able to catch about 100 GRBs per year, and XRT is able to follow them rapidly in the X-ray band and pinpoint their positions

¹Purple Mountain Observatory, Chinese Academy of Sciences, Nanjing 210008, China

²Department of Physics, Hebei Normal University, Shijiazhuang 050016, China

accurately. However, UVOT could only detect the optical afterglows in about 60% of them. Some of the detected optical afterglows are also weaker than those predicted by theoretical models. Those that have weaker or no optical afterglow are called optically dark GRBs (van der Horst et al. 2009).

The origin of dark GRBs is an open question in the research field of GRBs. Generally, the extinction by ambient dust grains is considered as the answer (Stratta et al. 2004; Schady et al. 2007), but the detailed theoretical implications are uncertain. The extinction curves measured for GRB afterglows are very diverse. Some of them are similar to that of the Small Magellanic Cloud (SMC), i.e., a steep extinction curve; some of them are similar to that of the Milky Way (MW), i.e., an extinction curve with significant extinction bump at ~ 2175 Å (Stratta et al. 2004); some of them are similar to that of a normal active galaxy with a flat extinction curve, i.e., gray extinction (Stratta et al. 2005; Chen et al. 2006). Obviously, the various extinction properties can not be fitted with the modeling sample of existing extinction curves. It is still a mystery how to infer the physical implications with different extinction curves. In this work, we adopt the latest algorithm for calculating dust physics and focus on the effect of dust extinction on GRB afterglows. By analyzing the influences of different physical parameters of dust grains on the extinction curves, we can reproduce various observed extinction curves and provide theoretical basis for the studies of dark GRBs and gray extinction.

2. PHYSICAL MECHANISM OF DUST EXTINCTION

Considering a spherical dust grain with radius a and complex refractive index \tilde{m} , and based on Mie theory (van de Hulst 1957), the extinction cross-section for the incident light with wavelength λ is

$$\sigma_{\text{ext}} = \frac{2\pi}{k^2} \sum_{n=1}^{\infty} (2n+1) \operatorname{Re} \{a_n + b_n\}, \qquad (1)$$

the scattering cross-section is

$$\sigma_{\text{sca}} = \frac{2\pi}{k^2} \sum_{n=1}^{\infty} (2n+1)(|a_n|^2 + |b_n|^2), \qquad (2)$$

and the absorption cross-section is $\sigma_{abs} = \sigma_{ext} - \sigma_{sca}$, where $k = 2\pi/\lambda$, and the scattering coefficients a_n and b_n are

$$a_n = \frac{\tilde{m}\psi_n(\tilde{m}x)\psi_n'(x) - \psi_n(x)\psi_n'(\tilde{m}x)}{\tilde{m}\psi_n(\tilde{m}x)\xi_n'(x) - \xi_n(x)\psi_n'(\tilde{m}x)},$$
(3)

$$b_n = \frac{\psi_n(\tilde{m}x)\psi_n'(x) - \tilde{m}\psi_n(x)\psi_n'(\tilde{m}x)}{\psi_n(\tilde{m}x)\xi_n'(x) - \tilde{m}\xi_n(x)\psi_n'(\tilde{m}x)},$$
(4)

where $x = ka = 2\pi a/\lambda$ is the dimensionless size parameter, and $\psi_n(x)$ and $\xi_n(x)$ are Riccati-Bessel functions.

Methods for numerical calculations based on Mie theory are mature now. Owing to the rapid development of computer science, the calculation of the infinite sums can be performed on popular PCs at present, instead of using supercomputers in the past. Numerical analyses indicate that the infinite series summation in Equations (1)-(4) can be approximated by the first $N = x + 4x^{1/3} + 2$ terms with a sufficiently high precision (Wiscombe 1980), where x is the dimensionless size parameter mentioned above. Currently, there are a few popular FORTRAN codes (Wiscombe 1980; Bohren & Huffman 1983), which can be very efficient (for a single calculation with $x \approx 10^3$, it only takes a couple of seconds on an Intel PC with a main frequency of 2.6 GHz), but is also numerically unstable and can be very time-consuming for multi-wavelength calculations, due to the lack of real-time adjustment of the precision, especially when x is very large (for X-rays and large dust grains, $x \gtrsim 10^5$). For the evaluation of absorption and scattering cross-sections over a broad bandpass and a wide size range of dust grains, multiple analytical approximations are usually adopted for interpolation (Wiscombe 1980). In order to study the properties of X-ray scattering and absorption by large dust grains, we make an extensive use of the latest MieSold code in the advanced language Mathematica which can make real-time adjustment of the precision with a sacrifice of the speed (for a single calculation with $x \approx 10^4$, it takes about 1 h on an Intel PC with a main frequency of 2.6 GHz). Nevertheless, the precision is greatly improved by self-adapting calculations over a much larger parameter space¹.

There are a variety of substances in the interstellar medium (ISM). The composition and optical properties of most dust grains can not be obtained directly by experiment or observation. They are mainly measured jointly by laboratory experiments, theoretical modelings and astronomical observations. At present, silicate and graphite are known as the two most important ingredients in ISM (Draine 2003b). Their optical properties have been systematically studied by Draine and his colleagues and the latest results on their complex refractive indices \tilde{m} have been summarized in Figure 1 (Draine & Lee 1984; Laor & Draine 1993; Li & Draine 2001; Draine 2003a). The optical properties of graphite are highly anisotropic, and the value of \tilde{m} is dependent on the angle included between the direction of electric field and the crystal axis. The "1/3 - 2/3" approximation is usually adopted in most evaluations, i.e., graphite is assumed as a mixture of two types of isotropic substances. Among them, 1/3 constituent resembles the graphite with the electric field parallel to the crystal axis and 2/3 constituent resembles the graphite with the electric field perpendicular

 $^{^1}$ Zimmer C, Aragon S R, Mie Scattering and Absorption from Bubbles and Spheres, Mathematica Journal, to be submitted.

to the crystal axis (Draine & Malhotra 1993). The X-ray edge absorption is taken into account in the results shown in Figure 1 (see $\text{Im}(\tilde{m})$, the imaginary part of \tilde{m}). The edge absorptions of silicate are quite abundant, including the multiple edge absorptions from Mg, Fe, Si and O, while graphite has only a K edge absorption between 282 and 310 eV (Draine 2003a).

Based on the above-mentioned optical properties of silicate and graphite, we can obtain their absorption and scattering cross-sections as functions of the grain size a and the energy of the incident light E by precise evaluations according to Mie theory. As shown in Figure 2, the results given by the MieSolid code (Rigorous Mie) are very consistent with those previously combined results based on multiple analytical approximations (Mie, Rayleigh-Gans [RG] and Geometric Optics [GO]) and have higher spectral resolution with better performance on the edge absorptions. The only flaw is that it is unstable in the ultraviolet and soft X-ray band when the grain size is larger than $1\,\mu\rm m$, which shall be tackled in the future code debugging. In this work, we adopt the existing approximative results for the unstable region via interpolation which will have negligible effect on the final results, since large grains in most standard dust models are deficient.

Our results (as in Figure 2) indicate that, when the typical grain size is small ($a < 0.1 \,\mu\text{m}$) absorption dominates the extinction with most of the incident energy transformed into ambient thermal energy. In this case, the scattering will be relatively weak, and it has been overlooked in previous works. On the contrary, when the typical grain size is large ($a > 0.1 \,\mu\text{m}$), the scattering dominates the extinction, especially the X-ray scattering will play an important role. As the grain is getting larger, the scattering is more effective. These results might have crucial implications for the studies of X-ray scattering in GRB afterglows (Shao & Dai 2007; Shao et al. 2008).

3. EXTINCTION OF GRB AFTERGLOWS

The size distribution of the dust grains around GRBs (Mathis et al. 1977) can be assumed obey a power law between (a_{\min}, a_{\max}) given by

$$\frac{\mathrm{d}N_i}{\mathrm{d}a}(a) = A_i \times N_{\mathrm{H}} a^{\beta} \quad (a_{\mathrm{min}} \le a \le a_{\mathrm{max}}), \tag{5}$$

where dN_i/da are the column densities per unit radius of silicate (i = 1) and graphite (i = 2), respectively, A_1 and A_2 are the coefficients that quantify their absolute column densities, N_H is the column density of hydrogen atoms, β is the dimensionless power-law index. Accordingly, the dust grain mass per unit hydrogen mass (Laor & Draine 1993), i.e., the equivalent metallicity is given by

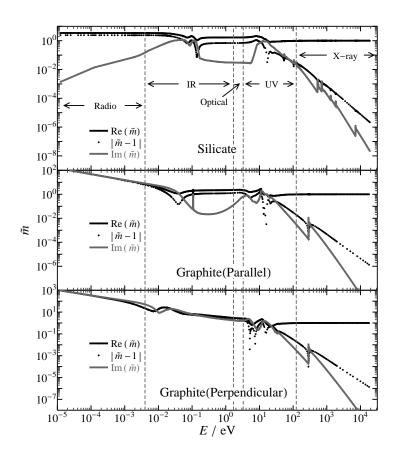


Fig. 1.— Complex refractive indices \tilde{m} of spherical silicate and graphite as functions of the energy of an incident photon. The real part and imaginary parts of the complex refractive indices represented by black and gray solid lines, respectively, and the values of $|\tilde{m}-1|$ that is frequently used in literatures are represented by dotted lines.

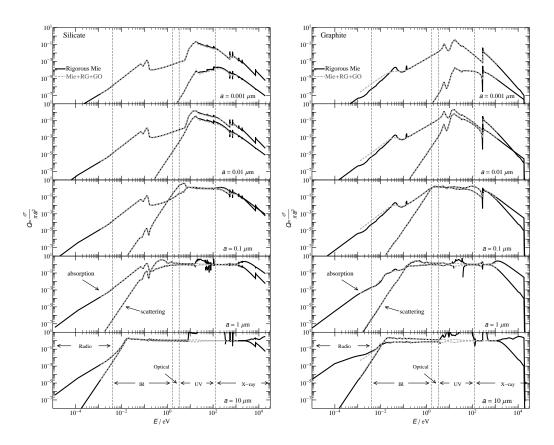


Fig. 2.— Variations of absorption and scattering cross sections of spherical silicate and graphite with frequency.

$$f_{\rm d} = \frac{4\pi}{3m_{\rm H}} \frac{a_{\rm max}^{\beta+4}}{\beta+4} \left[1 - \left(\frac{a_{\rm min}}{a_{\rm max}} \right)^{\beta+4} \right] \sum_{i} A_{i} \rho_{i} , \qquad (6)$$

where $\rho_1 = 3.3 \,\mathrm{g/cm^3}$ and $\rho_2 = 2.3 \,\mathrm{g/cm^3}$ are the mass densities of silicate and graphite, respectively, $m_{\rm H}$ is the mass of hydrogen atom. Here $f_{\rm d}$, A_1 and A_2 are not completely independent. Thereafter $f_{\rm d}$ and A_1/A_2 will be considered as two independent parameters. Meanwhile, the extinction optical depth can be given by

$$\tau(\lambda) = \int \sum_{i} \sigma_{\text{ext}}^{i}(\lambda) \frac{\mathrm{d}N_{i}}{\mathrm{d}a} \mathrm{d}a, \qquad (7)$$

and the extinction magnitude is $A(\lambda) = 1.086\tau(\lambda)$.

The GRB afterglows that are emitted by the shock-accelerated electrons in the relativistic outflow usually exhibit a power-law spectrum from the optical to X-ray band, which hereafter is assumed to be $F_{\nu} \propto \nu^{-1}$ (as shown by the gray solid line in Figure 3; Shao et al. (2010)). The column density of hydrogen atoms is the principal quantity that dominates the extinction from ultraviolet to soft X-ray band. As shown in Figure 3, from top to bottom, the solid, dotted, short-dashed and long-dashed lines represent that the values of $N_{\rm H}$ are 10^{20} cm⁻², 10^{21} cm⁻², $10^{21.6}$ cm⁻² and 10^{22} cm⁻², respectively. All the other physical parameters have the typical vales in ISM, where the metallicity $f_{\rm d}$ is 0.01, the ratio of silicate and graphite A_1/A_2 is 1 and the parameters for grain size distribution are $\beta=-3.5$, $a_{\rm min}=0.005\,\mu{\rm m}$ and $a_{\rm max}=0.25\,\mu{\rm m}$. In general, the column density of hydrogen atoms $N_{\rm H}$ determines the absolute amount of extinction. In some dense regions of the surrounding medium $N_{\rm H}$ could be very high (usually $N_{\rm H}>10^{22}$ cm⁻²), the optical to soft X-ray emissions from GRB afterglows would be severely attenuated.

Besides the column density of hydrogen atoms, many other factors will also affect the extinction curve (including the absolute amount of extinction and the profile of the extinction curve). Herein we mainly consider some key physical quantities: the ratio of silicate and graphite A_1/A_2 , the metallicity $f_{\rm d}$, parameters for dust grain size distribution β and $a_{\rm max}$. The impact of A_1/A_2 on the extinction curve is shown in Figure 4, where $A_1/A_2=0.6, 1.0, 1.6$ and 2.0 are represented by the solid, dotted, short-dashed and long-dashed lines, respectively. The other parameters also have the typical values, i.e., $f_{\rm d}=0.01, N_{\rm H}=10^{21.3}\,{\rm cm}^{-2}, \beta=-3.5, a_{\rm min}=0.005\,\mu{\rm m}$ and $a_{\rm max}=0.25\,\mu{\rm m}$. As revealed in the figure, A_1/A_2 mainly affects the extinction bump around 2175 Å, which has been known to be caused by small graphite grains (Draine & Malhotra 1993). Therefore, as A_1/A_2 increases, the extinction bump gets flatter. In general, the composition of dust grains has weak effect on the extinction curve and can not account for why we can observe evidently different extinction curves from GRB afterglows.

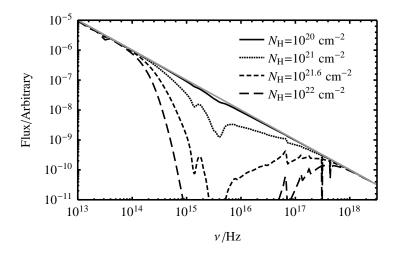


Fig. 3.— Extinction of GRB afterglow by circum-stellar dust grains with different column densities of hydrogen nuclei $N_{\rm H}$. Gray straight line represents the intrinsic spectrum of the afterglow.

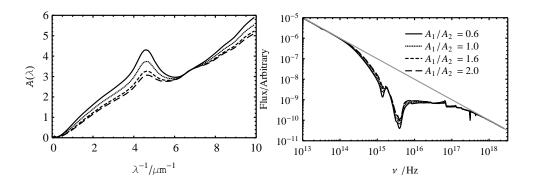


Fig. 4.— Extinction of GRB afterglow by circum-stellar dust grains with different relative abundances between silicate and graphite A_1/A_2 . Left panel is the extinction curve, and right panel is the attenuated afterglow spectrum. Gray straight line in the right panel represents the intrinsic spectrum of the afterglow.

The metallicity $f_{\rm d}$ has a great effect on the extinction curve. Being similar to the column density of hydrogen atom $N_{\rm H}$, which dominates the absolute amount of extinction, larger metallicity causes stronger extinction. As shown in Figure 5, $f_{\rm d}=0.001,\,0.004,\,0.007$ and 0.01 are represented by the solid, dotted, short-dashed and long-dashed lines, respectively. The other parameters also have their respective typical values, i.e., $A_1/A_2=1,\,N_{\rm H}=10^{21.3}\,{\rm cm}^{-2},\,\beta=-3.5,\,a_{\rm min}=0.005\,\mu{\rm m}$ and $a_{\rm max}=0.25\,\mu{\rm m}$. The ambient environment around a GRB is very complicated. There might be a high metallicity if the explosion occurs in the latter phase of the massive progenitor star which is an ideal place for the dust formation. This might be the leading cause of the severe extinction and the optically dark GRBs.

Obviously, as the computing results indicate, the power-law index of the dust grain size distribution β mainly determines the profile of the extinction curve. The chief reason is that dust grains with different sizes have different contributions to the extinction at different photon frequencies. This is governed by the physics of dust scattering, which is weakly affected by the ingredients of dust grains. As shown in Figure 6, $\beta = -3.5$, -2.5, -1.5 and -0.5 are represented by the solid, dotted, short-dashed and long-dashed lines, respectively. The other parameters also have the typical values, i.e., $f_{\rm d} = 0.01$, $A_{\rm 1}/A_{\rm 2} = 1$, $N_{\rm H} = 10^{21.3}\,{\rm cm}^{-2}$, $a_{\rm min} = 0.005\,\mu{\rm m}$ and $a_{\rm max} = 0.25\,\mu{\rm m}$. As the size of dust grains increases, the number of small dust grains decreases and the extinction bump around 2175 Å also becomes less evident. Another interesting feature is that β barely affects the optical extinction $A_{\rm V}$. This may explain why we can usually observe different extinction curves from GRB afterglows, but $A_{\rm V}$ is barely correlated with $N_{\rm H}$ (Schady et al. 2007). Our computing results indicate that difference of size distribution of dust grains might be the internal cause.

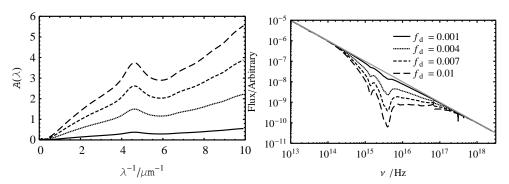


Fig. 5.— Extinction of GRB afterglow by circum-stellar dust grains with different metallicities. Left panel is the extinction curve, and right panel is the attenuated afterglow spectrum. Gray straight line in the right panel represents the intrinsic spectrum of the afterglow.

The upper limit for the size distribution of dust grains a_{max} is also an important pa-

rameter that determines the absolute amount of extinction. Being different from the abovementioned column density of hydrogen atom $N_{\rm H}$ and the metallicity $f_{\rm d}$, as $a_{\rm max}$ increases, the absolute amount of extinction decreases. As shown in Figure 7, the relations $a_{\rm max} = 10^{-0.5}$, 1, $10^{0.5}$ and $10 \,\mu{\rm m}$ are represented by the solid, dotted, short-dashed and long-dashed lines, respectively. The other parameters still have the typical values, i.e.,

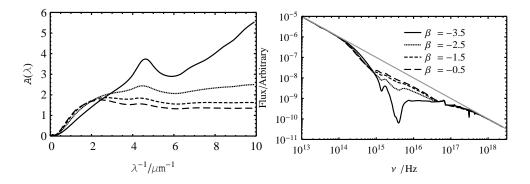


Fig. 6.— Extinction of GRB afterglow by circum-stellar dust grains with different indices of size distribution β . Left panel is the extinction curve, and right panel is the attenuated afterglow spectrum. Gray straight line in the right panel represents the intrinsic spectrum of the afterglow.

 $f_{\rm d}=0.01,\ A_1/A_2=1,\ N_{\rm H}=10^{21.3}\,{\rm cm}^{-2},\ \beta=-3.5$ and $a_{\rm min}=0.005\,\mu{\rm m}$. This phenomenon is due to an underlying assumption in our calculations that the total mass of the dust grains is conserved. Larger dust grains are formed by the aggregation of smaller ones. As the number of larger dust grains increase, the total number density of the dust grains will naturally decrease. Our computing results indicate that the absolute amount of extinction will remarkably decrease, and as the size of dust grain increases, the extinction curve will become flatter, causing gray extinction (Stratta et al. 2004; Li et al. 2008). Therefore, with β and $a_{\rm max}$ both varying, we would expect that the dust grains with typically larger sizes will cause weak extinction and have a flatter extinction curve, i.e., causing gray extinction. This explains why most observed optically bright afterglows exhibit flat extinction curves (Stratta et al. 2004). On the contrary, the dust grains with typically smaller sizes would cause more severe extinction, i.e., causing optically dark bursts, and have remarkably steeper extinction curves. Therefore, numerous computing results indicate that the discrepancy and evolution of the sizes of dust grains can have very crucial effects on the extinction curves of GRB afterglows.

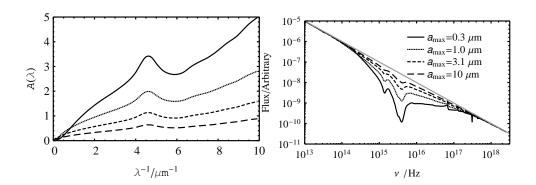


Fig. 7.— Extinction of GRB afterglow by circum stellar dust grains with different parameters of size distribution a_{max} . Left panel is the extinction curve, and right panel is the attenuated afterglow spectrum. Gray straight line in the right panel represents the intrinsic spectrum of the afterglow.

4. CONCLUSION

In this work, in order to study the effect of dust extinction on GRB afterglows, we carry out numerical calculations based on dust physics and explore the effects of various dust parameters on the extinction curves. We find that the medium density and the metallicity determine the absolute amount of extinction, and the parameters for the size distribution of dust grains β and a_{max} determine the profile of the extinction curve. When β is larger or a_{max} is larger, i.e., larger grains are more excessive, the extinction curve will be flatter with weak extinction. On the contrary, when β is smaller or a_{max} is smaller, i.e., smaller grains are more excessive, the extinction curve will be steeper with severe extinction, most likely causing the optical dark bursts. This may also explain why most bright afterglows tend to have flatter extinction curves. Therefore, the massive stellar birth of the GRB and its complex progenitor environment, should be the major cause of origin of the optical dark bursts and diverse optical afterglows. Observing and analyzing the extinction of afterglows would also be important to the studies of the GRB progenitors and their explosion mechanisms.

This work made use of the tabulated data of interstellar dust provided by B. T. Draine from Princeton University. We are grateful to S. Aragon from San Francisco State University for discussion on the MieSolid code and M. A. Caprio from University of Notre Dame for providing the updated LevelScheme package and enthusiastic technical support.

REFERENCES

Bohren, C. F., & Huffman, D. R. 1983, Absorption and Scattering of Light by Small Particles. New York: John Wiley & Sons, Inc., 475-482

Chen, S.-L., Li, A., & Wei, D.-M. 2006, ApJ, 647, L13

Draine, B. T. 2003a, ApJ, 598, 1026

Draine, B. T. 2003b, ARA&A, 41, 241

Draine, B. T., & Lee, H. M. 1984, ApJ, 285, 89

Draine, B. T., & Malhotra, S. 1993, ApJ, 414, 632

Gehrels, N., et al. 2004, ApJ, 611, 1005

Laor, A., & Draine, B. T. 1993, ApJ, 402, 441

Li, A., & Draine, B. T. 2001, ApJ, 554, 778

Li, Y., Li, A., & Wei, D.-M. 2008, ApJ, 678, 1136

Mathis, J. S., Rumpl, W., & Nordsieck, K. H. 1977, ApJ, 215, 425

Schady, P., et al. 2007, MNRAS, 377, 273

Shao, L., & Dai, Z.-G. 2007, ApJ, 660, 1319

Shao, L., Dai, Z.-G., & Mirabal, N. 2008, ApJ, 675, 507

Shao, L., Fan, Y.-Z., & Wei, D.-M. 2010, ApJ, 719, L172

Stratta, G., et al. 2004, ApJ, 608, 846

Stratta, G., et al. 2005, A&A, 441, 83

van de Hulst. 1957, Light Scattering by Small Particle. New York: John Wiley & Sons, Inc., 114-130

van der Horst, A. J., et al. 2009, ApJ, 699, 1087

Wiscombe, W. J. 1980, ApOpt, 19, 1505

This preprint was prepared with the AAS IATEX macros v5.2.